https://doi.org/10.1016/j.energy.2017.06.178

A two-stage framework for multiobjective energy management in distribution networks with a high penetration of wind energy

Bin Zhou[a,]*, Da Xu[a,]*, Ka Wing Chan[b], Canbing Li[a,]*, Yijia Cao[a], Siqi Bu[b]

[a] College of Electrical and Information Engineering, Hunan University, Changsha 410082, China

[b] Department of Electrical Engineering, The Hong Kong Polytechnic University, Hong Kong

Abstract

The integration of renewable energy sources (RESs) in distribution networks has brought great challenges to the volt/var management due to their intermittency and volatility. This paper proposes a two-stage energy management framework of distribution networks to facilitate the accommodation of high wind energy penetration. In the proposed framework, the volt/var management problem is formulated and decomposed as a two-stage energy scheduling optimization model with different time frames considering the uncertainties of wind energy and load forecasts. In the first stage, a scenario-based stochastic day-ahead scheduling model is formulated to optimize the 24-hour charging/discharging scheme of energy storage system (ESS) and power generation of diesel generator (DG) in order to minimize the expected operation cost. Based on the stochastic optimal scheduling results in the first stage, the second stage implements the multiobjective volt/var optimization (VVO) to determine the optimal real-time operation of volt/var control devices, considering the costs of adjusting the control devices (CACDs). The proposed method has been fully evaluated and benchmarked on a 69-bus distribution network under various operational scenarios to demonstrate its superiority on various performance metrics and further confirm its effectiveness and efficiency for distribution networks to accommodate a high penetration of wind energy.

Highlights

A multiobjective VVO is proposed for distribution networks with RESs.
A two-stage energy management framework is used to accommodate the wind energy.
ESS is utilized to reduce the network loss and maximize economic benefits.
ESS degradation cost and CACDs are considered in the volt/var management.

Keywords

Distribution networks, energy management, energy storage system, wind energy, volt/var optimization.

1. Introduction

Rapid development and advancement in smart grid technologies have enabled the renewable energy sources (RESs), especially the wind energy, to be grid-integrated in distribution networks with increasingly high penetration [1]. Annual wind energy production is growing significantly and has reached around 4% of worldwide energy consumption [2-4]. Now there are over two hundred thousand wind turbines (WTs) in onsite operation, with a total installed capacity of 432,000 MW at the end of 2015 [5]. Wind energy, as an alternative to the fossil fuels, is a clean and sustainable energy source without greenhouse gas emissions [6]. In general, distribution networks are normally operated as radial feeders, and various types of end-use loads are connected to the

*Corresponding author at: College of Electrical and Information Engineering, Hunan University, 410082 Changsha, China.
E-mail addresses: eedaxu@qq.com (D. Xu), licanbing@qq.com (C. Li), binzhou@hnu.edu.cn (B. Zhou).

feeders. Depending on the location of wind energy generation and the instantaneous mismatch between generation supply and load demand, the loads in the downstream of the connection points and even the total demand in the distribution network could be lower than the wind generation outputs. Therefore, the reverse power flows would be resulted as the energy is exported upstream along the feeders [7, 8]. Although wind energy may change the direction of branch power and thus reduce losses, if they are improperly managed, the reverse power flows from high penetration of wind energy can give rise to excessive losses [9]. The integration of high wind energy penetration would also cause a number of voltage quality concerns [10]. Since the X/R ratio of distribution lines is small, the wind energy has significant impact on the voltage profiles. Wind energy is accompanying with intermittency and volatility due to its dependency to the natural fluctuations, which would give rise to voltage fluctuations and deteriorate the voltage quality. This may ultimately lead to an increase in regulating times of on-load tap-changers (OLTCs) and capacitor banks, which accelerate the wear-and-tear of the volt/var control devices [11]. Consequently, it is critical to investigate an effective and feasible management scheme for distribution networks with high penetration of wind energy.

Volt/var optimization (VVO), referring to the regulation of voltage levels and reactive power over the feeders, is one of the most important control schemes in distribution networks [12, 13]. Various literatures have reported the application of VVO schemes in distribution networks. A multiobjective VVO model, with the objectives of the network losses, voltage deviations, and total energy costs, was proposed in [14], and a combinatorial multiobjective VVO model based on fuzzy logics was also reported in [15]. VVO was studied in [16, 17] and the exponential load model was used to represent the load-to-voltage functional relationship in the VVO problem. A model predictive control based VVO was proposed in [16] by scheduling the optimal tap positions of OLTCs and switch status of capacitor banks. Furthermore, a VVO framework to optimally control capacitor banks, voltage regulators and OLTCs was proposed in [18] to minimize the network loss and energy demand. However, the costs of adjusting the control devices (CACDs) have not been considered in these literatures yet.

So far, with the increase of wind energy penetration in smart distribution networks, the coordinated management of VVO and wind generation has become an emergent topic. The impacts of various RESs on the volt/var control performance have been analyzed in [19, 20]. A multi-timescale stochastic VVO was proposed in [21] to regulate the network voltages in the presence of uncertain RES outputs and load demands, and the multiobjective stochastic VVO methods for distribution networks with probabilistic characteristics of wind farms were studied in [22] and [23]. As the influence of active power from wind energy on voltage profile is much more than its reactive power [18, 20], the coordinated scheduling optimization of energy storage system (ESS) and volt/var control devices is necessary for the distribution networks with the high penetration of RESs. Hence, the volt/var management in this paper aims to coordinately schedule the active and reactive power in the distribution networks with high wind energy penetration.

The volt/var management in distribution networks is a challenging optimization problem due to the multiple objective functions, high-dimensional variables, highly constraints, coordination of various control devices with different time frames, and uncertainties of wind energy and load forecasts. This problem focuses on the coordinated optimization of daily charging/discharging scheme of ESS, outputs of diesel generator (DG), and scheduling scheme of volt/var control devices. However, it is inefficient for conventional methods to solve such a high dimensional and highly constrained problem while simultaneously minimizing the multiple operational objectives (i.e. network loss, voltage deviations (VD), CACDs, demand consumption, and the degradation cost of ESS). It should be pointed out that the dispatch of ESS and DG is based on the time-of-use (TOU) pricing and day-ahead wind and load scenarios, while the hourly scheduling of volt/var control devices is to dynamically update the real-time dispatch scheme and regulate the reactive power and voltage profile over the feeders. In this research, a two-stage multiobjective framework is proposed to solve the volt/var management problem of distribution networks. The proposed framework performs the stochastic economic generation scheduling of ESS and DG in the first stage to minimize the expected operation cost, including energy procurement cost, generation cost, ESS energy loss cost and degradation cost, and the second stage implements the multiobjective VVO to facilitate the accommodation of high wind energy penetration. The effects of the proposed approach under various penetration levels of wind energy on performance metrics have also been analyzed in the case study.

The rest of this paper is organized as follows: The mathematical models of distribution networks, WT, and end-use load are presented in Section 2. In Section 3, the proposed method is discussed and each stage is explained in detail. Comparative simulation studies under various wind energy penetrations are implemented in Section 4 to demonstrate the superiority of the proposed method. Finally, the paper is concluded in Section 5.

2. Problem Formulation

2.1 Distribution Network Model

For a typical radial distribution network as shown in Fig.1, there are N buses indexed by i =0, 1, ... , N. The complex power flows at each bus can be described as the following equations [16],

$$P_{i+1} = P_i - r_i \frac{P_i^2 + Q_i^2}{V_i^2} - p_{i+1} \tag{1}$$

$$Q_{i+1} = Q_i - x_i \frac{P_i^2 + Q_i^2}{V_i^2} - q_{i+1} \tag{2}$$

$$V_{i+1}^2 = V_i^2 - 2(r_i P_i + x_i Q_i) + (r_i^2 + x_i^2)\frac{P_i^2 + Q_i^2}{V_i^2} \tag{3}$$

$$p_i = p_i^{\mathrm{L}} - p_i^{\mathrm{G}}, \quad q_i = q_i^{\mathrm{L}} - q_i^{\mathrm{G}} \tag{4}$$

where V_i is the voltage of bus i; the apparent power from bus i to bus $i+1$ is represented with $S_i = P_i + jQ$; the load demand at bus i is represented with ; the complex impedance in the line between bus i to bus is represented with $z_j = r_j + jx_j$; p_i^{L} and q are the active and reactive loads at bus i, respectively; is the active power generated by the RESs and DG units at bus i; is the reactive power generated by the RESs, DG units and reactive power compensation devices at bus i.

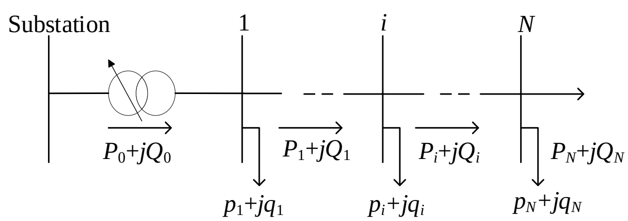

Fig.1 Schematic diagram of a radial distribution network

2.2 Wind Turbine Model

The power curve of a WT depicts the electrical power output of wind generation as a function of wind velocity [19]. As shown in Fig. 2, a WT starts generating power at the cut-in wind speed and reaches its rated power at the rated speed v_{r}. Since then, the power output remains the constant at the rated power till the cut-off wind speed v_{out} with the increase of wind velocity w. In this paper, a typical piecewise linear method in [19] is adopted to approximate the nonlinear power curve of WTs, as formulated in (5),

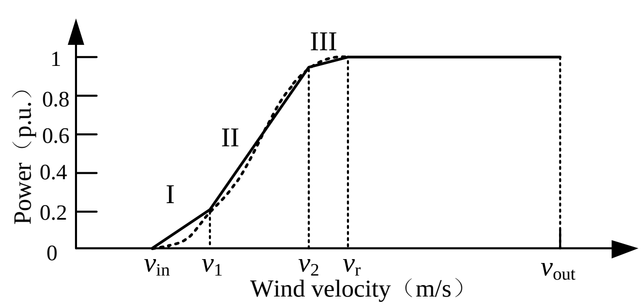

Fig.2 Power curve of WT (dotted) and piecewise linear approximation (solid)

$$P_{\mathrm{WT}} = P_{\mathrm{W}} \times \begin{cases} r_1(w - v_{\mathrm{in}}), & v_{\mathrm{in}} \le w \le v_1 \\ r_1(v_1 - v_{\mathrm{in}}) + r_2(w - v_1), & v_1 \le w \le v_2 \\ r_1(v_1 - v_{\mathrm{in}}) + r_2(v_2 - v_1) + r_3(w - v_1), & v_2 \le w \le v_r \\ 1, & v_r \le w \le v_{\mathrm{out}} \\ 0, & \text{otherwise} \end{cases} \tag{5}$$

where P_{W} is the rated wind power; is the wind speed; r_i and are the slope and wind speed break-point of the piece of wind power curve, respectively; is the rated wind speed; and are the cut-in speed and cut-out speed, respectively. Here, the parameters in (5) are assigned the values with following [19]: r =0.2/$(v_1 - v_{ci})$, r_2=(0.96-0.2)/), =(1-0.96)/$(v_r - v_2)$, v_1 =7 m/s, v_2 =12 m/s, v_r =14 m/s, v_{in} = 4 m/s, and = 25 m/s.

2.3 End-Use Load Model

The end-use load model describes the load behaviors with the change of nodal voltage. In most previous studies of distribution networks, many load models have been developed, among which, polynomial and exponential load models have been widely used to represent the load-to-voltage relationship [16-18]. Here, the exponential load model can be formulated as,

$$P_{Li} = P_{0i}\left(\frac{V_i}{V_{0i}}\right)^{p_i} \tag{6}$$

$$Q_{Li} = Q_{0i}\left(\frac{V_i}{V_{0i}}\right)^{q_i} \tag{7}$$

where P_{Li} and Q_{Li} are the active and reactive load demand at bus i, respectively; and Q_{0i} are the active and reactive load demand at rated voltage and frequency at bus i, respectively; and V_i are the rated voltage and voltage magnitude at bus i, respectively; p_i and are the constant parameters of the exponential load model whose values are determined by load compositions. Usually, the end-use loads of distribution network can be mainly characterized as residential, commercial and industrial loads, and their corresponding parameter values are shown in Table 1 [24]. It should be emphasized that a feeder contains more than one load type, and thus a load-mix requires to be implemented, as discussed in Section 4.

Table 1 Parameters of different exponential load models

Lode type		
Residential	1.04	4.19
Commercial	1.50	3.15
Industrial	0.18	6.00

2.4 Uncertainty Characterization

The day-ahead optimal scheduling of volt/var management for distribution networks with a high penetration of wind energy is performed based on the load forecasting, TOU and wind energy forecasting. The forecasting data of load profile of each bus in this distribution network is obtained with Gaussian mixture model in [25], and the wind speed forecast follows the Weibull distribution function using the Weibull constant and the average wind speed [23]. Due to the intermittent and randomness nature of the RESs, their generation outputs will be highly stochastic and difficult to accurately predict. The uncertainty also exists in the load because of the stochastic variations of energy usage behaviors and weather conditions. In this study, these sources of uncertainty are modeled based on the Monte Carlo scenarios [23]. The Monte Carlo simulation is adopted to generate scenarios in which each scenario represents a possible status with wind speed and load forecasting inaccuracies. The parameters in the Monte Carlo simulation are probability distribution functions for load and wind speed forecast errors. Here, the load forecast error is assumed to follow a truncated normal distribution in [26], in which the mean is the hourly load forecast and the standard deviation is 5% of the mean, as follows,

$$f(x)=\begin{cases}0 & x<\mu-3.5\sigma \text{ or } x>\mu+3.5\sigma \\ \dfrac{1}{\alpha\sqrt{2\pi}\sigma}e^{-(x-\mu)^2/2\sigma^2} & \mu-3.5\sigma\le x\le\mu+3.5\sigma\end{cases} \tag{8}$$

where $\alpha=\int$ dx; x indicates the load forecast error; and are the mean and standard deviation of the normal distribution, respectively.

The wind speed forecast error is characterized by the auto-regressive moving average (ARMA) [26], and a lower order ARMA (1,1) time series is defined to simulate the wind speed data as,

$$X(t)=\alpha X(t-1)+Z(t)+\beta Z(t-1) \tag{9}$$

where $X(t)$ is the wind speed forecast error in the tth hour forecast; and are constant parameters, and $Z(t)$ is the random Gaussian variable with mean equal to zero and standard deviation .

The scenario tree can be formed by several scenarios generated from historical forecasting data. If there are u scenarios, each scenario can be considered as a path with a possibility of $1/u$. Since the computational requirement for solving the scenario-based scheduling problems would increase rapidly with the number of scenarios, a scenario reduction technique in [21] is adopted for the tradeoff between the computation efficiency and the modeling accuracy. After the implementation of scenario reduction, S scenarios can be obtained, and each scenario expresses a possible day-ahead profile, in which Pr_s is assigned as the weight to reflect the possibility of occurrence of each scenario. The sum of the probabilities for all scenarios is equal to 1, that is $\sum Pr_s=1$.

3. Proposed Two-Stage Framework

The voltage profile and power flow will be affected by the integration of high wind energy penetration [19]. The interaction between the dispatchable active/reactive power devices and wind energy is required for the improvements of various operational objectives. As the frequent actions of volt/var control devices could cause voltage fluctuation and wear-and-tear of management equipment in distribution networks, CACDs are considered and formulated into the objective function of conservation voltage reduction. Furthermore, the ESS degradation cost is also considered in this model as the state of charge (SOC) and ambient temperature could cause considerable degradation to ESS [27]. It should be noted that the grid integration of ESS in distribution networks with large-capacity wind energy is economically feasible, and the ESS model proposed in [27] is applied in this study. In mathematical terms, the volt/var management problem can be formulated as the following multiobjective optimization model,

$$\begin{aligned}&\text{Min} \quad f_i(X)\\ &X=[SOC_1,...,SOC_{N_E},P_1,...,P_{N_D},Q_1,...,Q_{N_D},T_1,...,T_{N_B},Q_1,...,Q_{N_C}]\\ &\text{s.t.} \quad \begin{cases} q_k(X)=0, & k=1,2,...,M_{\text{eq}}\\ g_j(X)\le 0, & j=1,2,...,M_{\text{ineq}}\end{cases}\end{aligned} \tag{10}$$

where f_i represents the ith objective function, such as economic cost, energy conservation and VD; M_{eq} and M_{ineq} are the number of equality and inequality constraints, respectively; X is a set of decision variables including the SOC of ESSs, outputs of DGs, tap positions of OLTCs, and reactive power outputs of shunt capacitor banks; N_E, N_D, N_B, and N_C are the numbers of ESSs, DGs, OLTCs, and shunt capacitors, respectively. The scheduling problem in (10) is a multi-horizon and high dimensional optimization problem with multiple objectives, wind energy and load forecasting uncertainties, and hence a two-stage scheduling framework is proposed here to solve this optimization problem. The first stage is to optimize the day-ahead stochastic generation scheduling of ESSs and DGs, and the VVO is implemented in the second stage for the efficient conservation voltage reduction. In this model, the reverse injections to the main grid is allowed without any rejection, and all active power import/export from/to the distribution companies, as well as the ESS energy loss, will be paid with the same price model [28].

3.1 The First Stage

The scenario-based stochastic day-ahead economic generation scheduling is implemented in this stage to optimize the charging/discharging scheme of ESS and generation of DGs based on the generated wind and load scenarios. The total expected operation cost, C_O, in this model can be formulated as the sum of expected operation cost of all day-ahead scenarios, as follows,

$$\mathrm{Min}\ \ C_\mathrm{O} = C_\mathrm{EC} + C_\mathrm{DG} + C_\mathrm{ESS} \tag{11}$$

where

$$C_\mathrm{EC} = \sum_{s=1}^{N_s} Pr_s \left\{ \sum_{t=1}^{T} C_t^\mathrm{e} \cdot (P_t^\mathrm{L} - P_{t,s}^\mathrm{DG} - P_{t,s}^\mathrm{WT} - \sum_{i=1}^{N_E} (P_{i,t,s}^\mathrm{dis} - P_{i,t,s}^\mathrm{ch})) \right\} \tag{12}$$

$$C_\mathrm{DG} = \sum_{s=1}^{N_s} Pr_s \left\{ C_\mathrm{f} \cdot (\sum_{i=1}^{N_D} \sum_{t=1}^{T} P_{i,t,s}^\mathrm{DG}) + \sum_{k=1}^{K} v_k \cdot (\sum_{i=1}^{N_D} \sum_{t=1}^{T} P_{i,t,s}^\mathrm{DG}) \cdot (V_k + V_k') \right\} \tag{13}$$

$$\begin{aligned} C_\mathrm{ESS} = & \sum_{s=1}^{N_s} Pr_s \left\{ \sum_{t=1}^{T} C_t^\mathrm{e} \cdot \left[\sum_{i=1}^{N_E} (1-\eta_i^\mathrm{ch}) \cdot P_{i,t,s}^\mathrm{ch} + \sum_{i=1}^{N_E} (1/\eta_i^\mathrm{dis} - 1) \cdot P_{i,t,s}^\mathrm{dis} \right] \right\} + \\ & \sum_{s=1}^{N_s} Pr_s \left\{ \sum_{t=1}^{T} \sum_{i=1}^{N_E} (P_{i,t,s}^\mathrm{ch} + P_{i,t,s}^\mathrm{dis}) \frac{C_i^\mathrm{E} \cdot L_i^\mathrm{R}}{k_i \cdot [a_i(1-SOC_{i,t,s}) + b_i] \cdot \exp(\alpha_i T_{i,t}) \cdot E_i^\mathrm{R} \cdot (1 - SOC_i^\mathrm{ref})} \right\} \end{aligned} \tag{14}$$

where C_EC in (12) describes the expected procurement cost of energy supplied from main grid; in (13) represents the expected fuel cost of the energy generated by DGs and the environmental cost of various pollutant emissions; in (14) represents the expected energy loss cost and degradation cost of ESS; The first term in (14) represents the energy loss cost due to battery charging/discharging efficiency, and the second term expresses the cost of equipment degradation because of the wear and tear caused by frequent charging and discharging of batteries; is the number of day-ahead scenarios and s is the index of scenarios; is the number of total dispatching hours; is the unit price of energy supplied by distribution companies at the hour; P is the generation of wind energy at the hour in scenario s; is the total demand consumption during the hour; v_k, , and are emission factor, environmental value, and penalty of the type of pollutant respectively, and is the number of pollutant types; represents the unit fuel price of DGs, and is the generation of the DG at the hour in scenario s; $P_{i,t,s}^\mathrm{ch}$ and are the charging and discharging energy of the th ESS at the t hour in scenario s, respectively; η_i^ch and are the charging and discharging efficiency of ESS of the ESS, respectively; is the capital cost of the ith ESS including replacement labor; L_i^R is the rated cycle life of the ESS estimated by manufactures under rated ambient temperature and SOC; SOC_i^ref and $SOC_{i,t,s}$ are the reference SOC and the current SOC of the ith ESS at the hour in scenario s, respectively; k_i and are coefficients of cycle life of the ESS which are dependent on the temperature; a_i and b_i are coefficients of cycle life of the ith ESS which are dependent on the SOC; $T_{i,t}$ is the ambient temperature in degree centigrade of the ith ESS at the tth hour; E_i^R is the total energy storage capacity of the ith ESS.

The stochastic generation scheduling problem in the first stage is subjected to the following constrains:

1) Energy storage constraints: Energy loss would occur in the charging/discharging energy conversion of ESS,

$$SOC_{i,t+1,s} - SOC_{i,t,s} - \frac{\eta_i^\mathrm{ch} P_{i,t,s}^\mathrm{ch}}{E_i^\mathrm{R}} + \frac{P_{i,t,s}^\mathrm{dis}}{\eta_i^\mathrm{dis} E_i^\mathrm{R}} = 0 \qquad i = 1, 2, ..., N_E \tag{15}$$

2) SOC constraints: The SOC should be limited to avoid the overcharging and overdischarging of ESS, as follows,

$$SOC_{i,\min} \le SOC_{i,t,s} \le SOC_{i,\max} \qquad i = 1, 2, ..., N_E \tag{16}$$

where and are the lower bound and upper bounds of the ESS, respectively.

3) Charging/discharging constraints: Since the fast charging/discharging rate would degrade the performance of ESS and thus shorten the lifespan, the charging/discharging energy should be limited as follows,

$$P_{i,t,s}^\mathrm{ch} \le P_{i,\max}^\mathrm{ch} \cdot \delta_{t,s} \qquad i = 1, 2, ..., N_E \tag{17}$$

$$P_{i,t,s}^{\text{dis}} \le P_{i,\max}^{\text{dis}} \cdot \varphi_{t,s} \qquad i = 1,2,...,N_E \tag{18}$$

$$\delta_{t,s} + \varphi_{t,s} \le 1 \tag{19}$$

where $\varphi_{t,s}$ and δ are binary variables to represent the state of ESS energy flow (i.e., charging or discharging) during the hour in scenario s; and $P_{i,\max}^{\text{dis}}$ are the allowed maximum charging and discharging energy of the ESS for each hour, respectively.

4) DG output constraints: The output of DG should be limited within its maximum and minimum generation outputs,

$$P_{i,\min}^{\text{DG}} \le P_{t,i,s}^{\text{DG}} \le P_{i,\max}^{\text{DG}} \qquad i = 1,2,...,N_D \tag{20}$$

where and are the maximum and minimum generation outputs of the DG for each hour, respectively.

3.2 The Second Stage

In this stage, the multiobjective VVO is implemented to dispatch the volt/var control devices, outputs of ESS and DG based on the scheduled results solved in the first stage and the real-time data. Moreover, the utilization of SCADA/DMS and the growing penetration of advanced metering infrastructure can provide sufficient valuable real-time information for utilities to implement the proposed VVO scheme [29]. Consequently, the optimization objectives of VVO, including the total energy consumption and VD, can be formulated as follows,

$$\text{Min} \quad P_{\text{S}} = P_{\text{Loss}} + P_{\text{L}} + P_{\text{CACD}} \tag{21}$$

$$\text{Min} \quad \text{VD} = \sum_{i=1}^{N} \left| \frac{V_i^* - V_{i,t}}{V_i^*} \right| \tag{22}$$

where

$$P_{\text{Loss}} = \sum_{k=1}^{N_L} G_{k,t} (V_{i,t}^2 + V_{j,t}^2 - 2|V_{i,t}||V_{j,t}|\cos\delta_{ij,t}) \tag{23}$$

$$P_{\text{L}} = \sum_{i=1}^{N} p_{0i} (\frac{V_{i,t}}{V_{0i}})^{\alpha_i} \tag{24}$$

$$P_{\text{CACD}} = C_B \sum_{i=1}^{N_B} \Delta u_{B_i} + C_C \sum_{i=1}^{N_C} \Delta u_{C_i} \tag{25}$$

where P_{Loss} in (23) is the network loss; in (24) represents the total end-use loads; in (25) is the costs of adjusting OLTCs and shunt capacitor banks; VD represents the voltage deviation; and N are the number of distribution lines and buses; and are nominal voltage and voltage magnitude of the bus at the tth hour, respectively; is the conductance of the branch line connecting the ith and the jth bus; is the voltage angle difference between the th and the j bus; C and are the unit adjustment cost of OLTCs and shunt capacitor banks, respectively; Δu_{B_i} and are the operating times of OLTC and capacitor bank, respectively.

The objective functions in the second stage are subjected to the following constrains:

1) Power-flow equality constraints: The load flow equality constraints include the active and reactive power balance at each bus, as follows,

$$P_t^{\text{S}} + P_{i,t}^{\text{DG}} + P_{i,t}^{\text{WT}} + P_{i,t}^{\text{dis}} - P_{i,t}^{\text{ch}} - P_{i,t}^{\text{L}} = P_{i,t}(\theta, V, tap) \qquad i = 1,2,...,N \tag{26}$$

$$Q_t^{\text{S}} + Q_{i,t}^{\text{DG}} - Q_{i,t}^{\text{L}} + Q_{i,t}^{\text{C}} = Q_{i,t}(\theta, V, tap) \qquad i = 1,2,...,N \tag{27}$$

where $P_{i,t}^{\text{DG}}$ and are the active and reactive power of the DG at the bus during the hour, respectively; is the reactive power compensation at the bus from shunt capacitor banks at the hour; and are active and reactive power supplied from main grid during the hour, respectively; is the output of WTs at the th bus during the t hour; $P_{i,t}^{\text{L}}$ and are the active and reactive loads at the bus during the hour, respectively; and

$Q_{i,t}(\theta, V, tap)$ are the active and reactive power injection at the ith bus during the tth hour.

2) OLTC constraints: The tap position of transformer can be stepwise regulated, and should be bounded within its minimum and maximum limits, as follows,

$$tap_{i,\min} \le tap_{i,t} \le tap_{i,\max} \qquad i = 1, 2, ..., N_B \tag{28}$$

where $tap_{i,\max}$ and $tap_{i,\min}$ are the maximum and minimum tap positions of the ith OLTC for each hour, respectively.

3) Capacitor bank constraints: The VAR output generated by capacitor can be stepwise changed, and should also be within its lower and upper limits, as follows,

$$Q_{i,\min}^{\mathrm{C}} \le Q_{i,t}^{\mathrm{C}} \le Q_{i,\max}^{\mathrm{C}} \qquad i = 1, ..., N_C \tag{29}$$

where $Q_{i,\max}^{\mathrm{C}}$ and $Q_{i,\min}^{\mathrm{C}}$ are the maximum and minimum VAR outputs of the ith capacitor bank for each hour, respectively.

4) DGs reactive power constraints: The reactive power output should be limited by the capacity limitation of DG, as follows,

$$Q_{i,\min}^{\mathrm{DG}} \le Q_{i,t}^{\mathrm{DG}} \le Q_{i,\max}^{\mathrm{DG}} \qquad i = 1, ..., N_D \tag{30}$$

where $Q_{i,\max}^{\mathrm{DG}}$ and $Q_{i,\min}^{\mathrm{DG}}$ are the maximum and minimum reactive power of the ith DG for each hour, respectively.

5) Distribution branch constraints: The apparent power flow of the kth branch line connecting bus i and j should be limited within its loading limit to avoid overloading,

$$\left| S_{ij,t} \right| \le S_{ij,\max} \qquad k = 1, 2, ..., N_L \tag{31}$$

where $S_{ij,t}$ and $S_{ij,\max}$ are the absolute power over distribution lines and the maximum transmission power between bus i and bus j, respectively.

6) Nodal voltage constraints: The voltage magnitude of each bus shall be constrained between its lower and upper limits,

$$V_{i,\min} \le V_{i,t} \le V_{i,\max} \qquad i = 1, 2, ..., N \tag{32}$$

where $V_{i,\min}$ and $V_{i,\max}$ are the minimum and maximum allowable voltage of the ith bus, respectively.

7) Power factor constraints: The substation should be operated with a limited power factor as follows,

$$PF_{\min} \le PF_t^{\mathrm{sub}} \le PF_{\max} \tag{33}$$

where $PF_{\max}$, $PF_{\min}$, and PF_t^{sub} are the maximum, minimum and current substation power factor, respectively.

8) DG output and ESS charging/discharging constraints: The output of DG and the charging/discharging rate of ESS should be bounded within their maximum and minimum limits, as formulated in (15)-(20).

Fig 3 illustrates the flowchart for implementation process of the proposed two-stage scheduling framework. In this study, the energy management in the first stage is optimized by the BONMIN solver on GAMS [30], and the multiobjective differential evolution (MODE) algorithm [31] with MATLAB is adopted to solve the bi-objective VVO problem in the second stage. The implementation framework in Fig 3 can be achieved using GDXMRW for the interfacing GAMS and MATLAB [30]. For the resulting multiobjective solution set, the fuzzy logic based decision making method in [32] is applied to identify the best compromise solution from the Pareto optimal frontier. In this multi-criteria decision making method, the ith objective function value of a solution in the Pareto-optimal set, F_i, is represented by a membership function μ_i defined as,

$$\mu_i = \begin{cases} 1 & F_i \le F_{i,\min} \\ \dfrac{F_{i,\max} - F_i}{F_{i,\max} - F_{i,\min}} & F_{i,\min} \le F_i \le F_{i,\max} \\ 0 & F_i \ge F_{i,\max} \end{cases} \tag{34}$$

where $F_{i,\max}$ and $F_{i,\min}$ are the maximum and minimum values of the ith VVO objective function, respectively. For the kth nondominated solution, the normalized membership value $\mu(k)$ is formulated as follows,

$$\mu(k)=\frac{\sum_{i=1}^{n}\mu_i(k)}{\sum_{j=1}^{m}\sum_{i=1}^{n}\mu_i(j)} \tag{35}$$

where m indicates the number of nondominated solutions in the resulting solution set, and n is the number of VVO objective functions. Consequently, the best compromise solution can be derived from the solution with maximal normalized membership value.

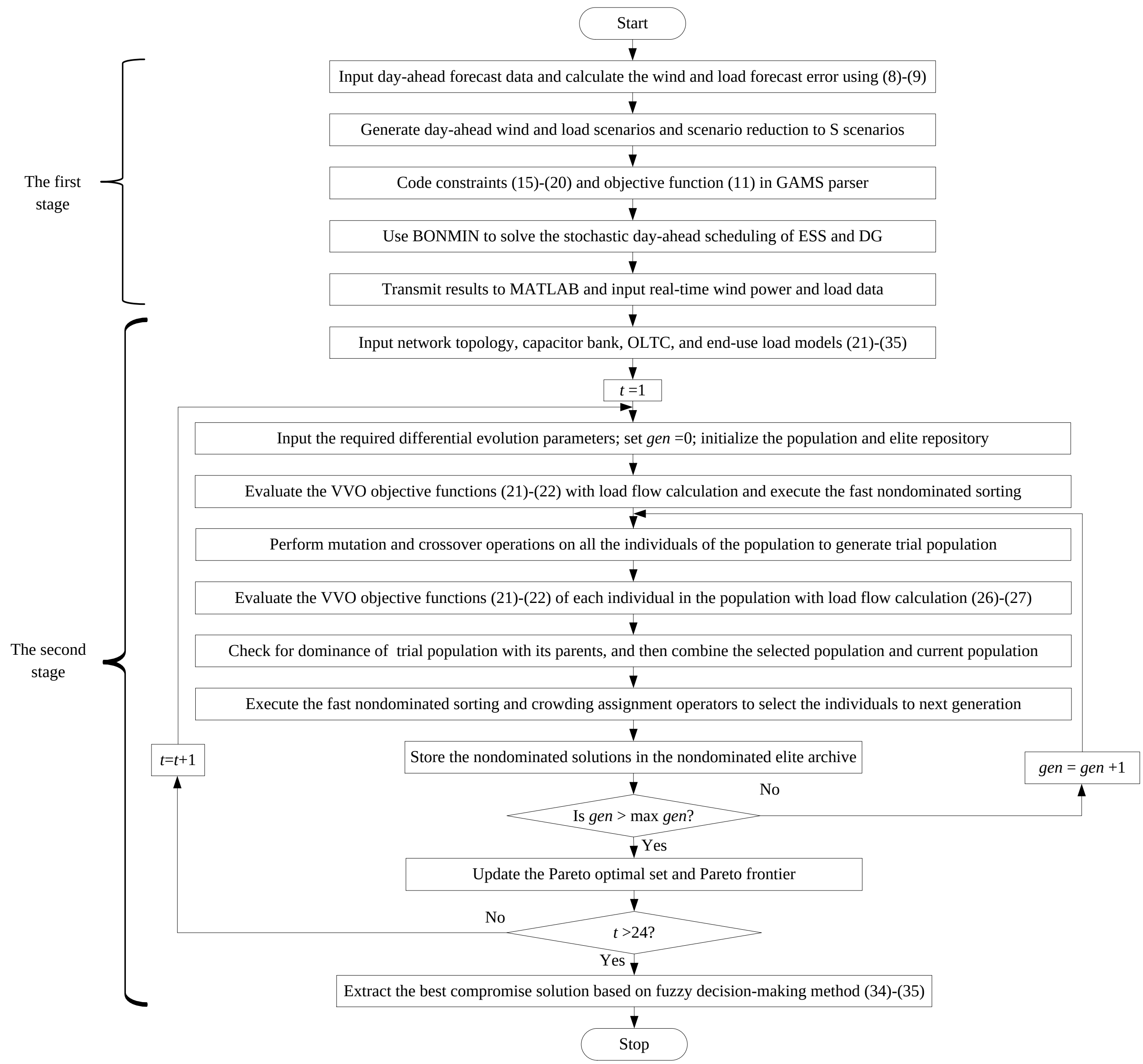

Fig.3 Flowchart of the proposed two-stage energy management framework

4. Case Study

The proposed two-stage scheduling scheme is tested on a modified 69-bus distribution network, as shown in Fig. 4, to solve the multiobjective volt/var management problem. While the detailed network topology and data are given in [33], this scheduling problem has 9 dispatchable variables within each decision cycle, including the active/reactive power outputs of a DG installed at bus 12, the tap position of a OLTC at the substation, the charging/discharging schemes of 2 ESSs installed at buses 2 and 51, and 4 shunt capacitors installed at buses 22, 30, 39 and 63. Here, the rated capacity of the DG is 1 MW and its pollutant emission parameters are obtained from [34]. The minimum generation output of DG is 0.2 MW, and the unit fuel price C_{f} is 145 \$/MWh [34]. The OLTC ratios are constrained in the range of 0.95-1.05 with a step size of 0.0125, and all the VAR outputs of capacitors are within the interval of 0-0.5 with a step size of 0.1 MVar [18]. The cost coefficients of CACDs, C_B and C_C, are set to 10 kW and 6 kW per time, respectively [35]. The rated capacities of WTs installed at buses 25, 41, 48, 53 and 69 are 0.7 MW. The lead-acid battery in [27] is selected as the ESS in this study. The rated capacities of batteries are 1 MWh and the maximum charging/discharging rate is limited to 20% of their rated capacity [27]. In order to obtain prolong battery lifespan, the lower bound, initial value and upper bounds of SOC are set to 0.3, 0.3 and 0.9, respectively. The charging/discharging efficiency and the coefficients of cycle life in battery degradation cost are obtained from [27]. Besides, the nodal voltage limits, $V_i^{\max}$ and $V_i^{\min}$, are set to 1.06 and 0.94 p.u., respectively. The network power factor limits, $PF_{\max}$ and $PF_{\min}$, are set to 0.99 lag and 0.96 lag, respectively [17]. The network base voltage and base power are 12.66 kV and 1 MVA.

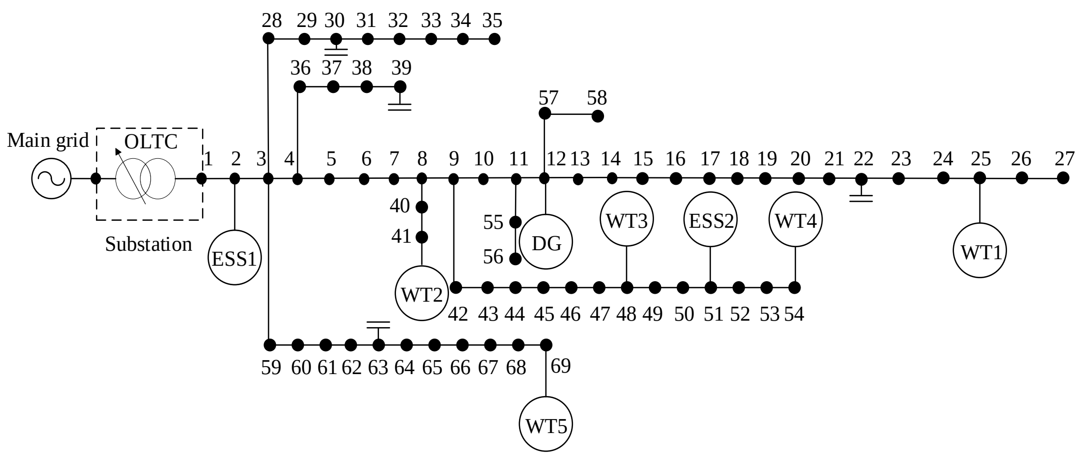

Fig. 4 Network topology of the modified 69-bus distribution network

Table 2 Nodal load types

Load type	Residential	Industrial	Commercial
Bus No.	1-27	28-39, 59-69	40-58

In the 69-bus distribution network as shown in Fig. 4, various types of exponential end-use load models in different buses, including residential, industrial, commercial loads, are listed in Table 2. Here, 200 day-ahead scenarios are generated with the scenario tree method in Section 2.4, and only 5 scenarios are retained after scenario reduction operation, as shown in Fig. 5(a)-(c). The curves of wind energy and load demand on a typical weekday are shown in Fig. 6(a)-(c). Furthermore, the power tariff model of TOU is used for charging different rates throughout the day, with the TOU pricing settings from [36], as shown in Fig. 6(d).

In this case study, the following five schemes are considered for the in-depth comparisons and analyses. The proposed volt/var management is a highly nonlinear, non-differential, high-dimensional and multimodal Pareto optimization problem and thus can be solved with a highly effective and classical method, MODE [31]. The parameter settings of MODE have been heuristically well-tuned through a number of comparative studies and simulations. Thus, the population size and maximum number of algorithm iterations in the Schemes 1-5 are set to 50 and 100, and the population size and maximum number of iterations in Scheme 6 are set to 500 and 500, respectively. Besides, the algorithm crossover and mutation probabilities in all the schemes are set to 0.5 and 0.9, respectively [31]. Ten independent runs of MODE algorithm in each scheme have been carried out, and the resulted sets of nondominated solutions are then combined and ranked by dominance comparisons to yield the resulting Pareto frontier of each scheme.

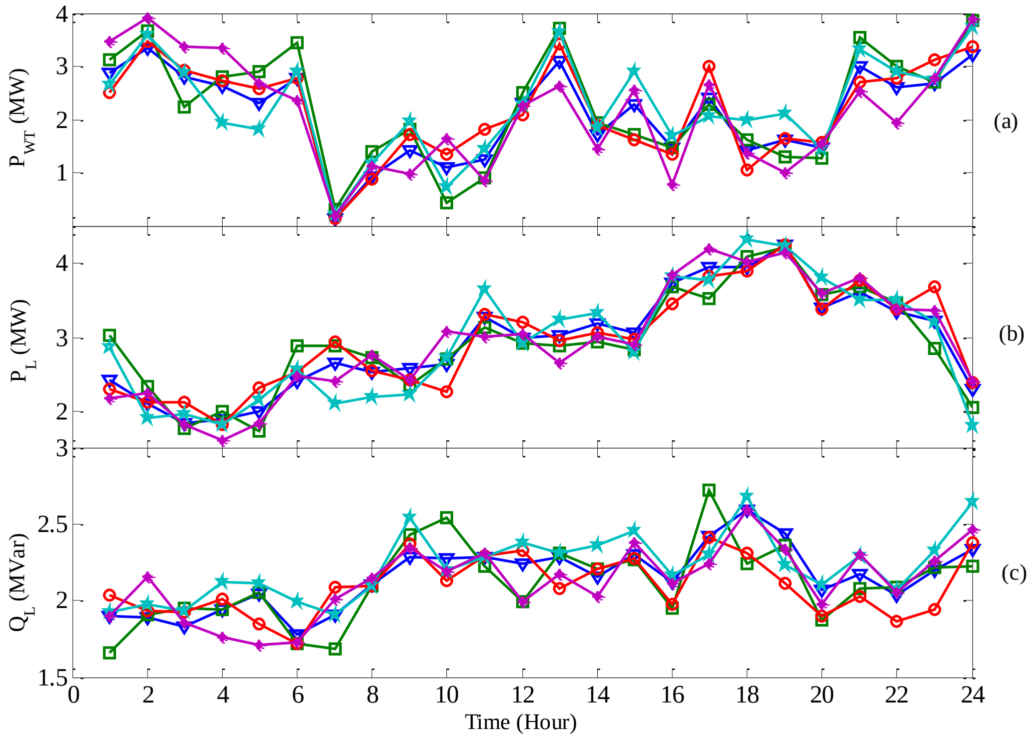

Fig. 5 The curves of day-ahead scenarios of wind energy and load demand:
(a) Total wind energy generation; (b) Total active load demand; (c) Total reactive load demand.

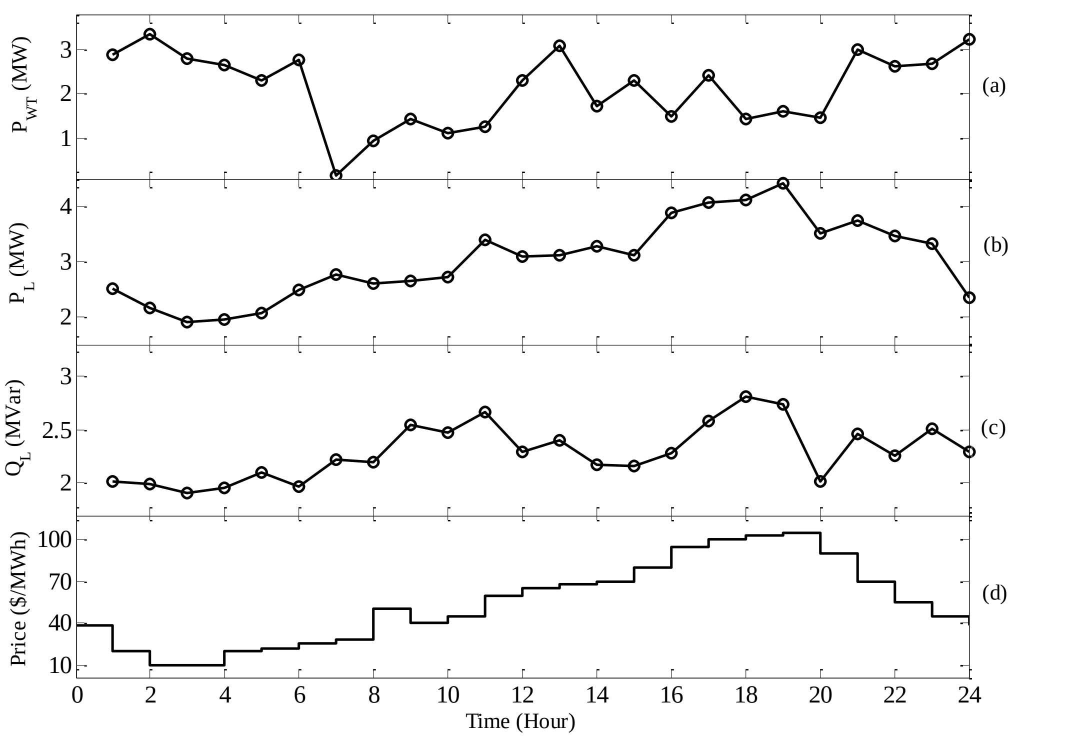

Fig. 6 The curves of real-time data of wind energy, load demand, and power price:
(a) Total wind energy generation; (b) Total active load demand; (c) Total reactive load demand; (d) TOU power price.

1) Scheme 1: This scheme is the proposed two-stage scheduling scheme as mentioned in Section 3;

2) Scheme 2: On the basis of the two-stage method in Scheme 1, the ESS is not scheduled in the optimization model;

3) Scheme 3: On the basis of the two-stage method in Scheme 1, the ESS is considered and scheduled in the optimization model of this scheme, and the battery degradation cost and energy loss cost in (14) is not considered in the objective function (11) for the first stage;

4) Scheme 4: On the basis of the two-stage method in Scheme 1, CACDs in (25) are not considered in the objective function (21) for the second stage;

5) Scheme 5: This scheme implements the volt/var management to simultaneously optimize the first stage and the second stage based on the real-time load and wind generation data for each hour, determining the optimal operations of ESSs, DG, OLTC, and shunt capacitor banks for the three objective functions in (11), (21), and (22);

6) Scheme 6: This scheme implements the 24-hour sequential optimization of volt/var management to jointly optimize the first stage and the second stage based on the forecasting load and wind generation data for the three objective functions in (11), (21), and (22).

Table 3 Comparative performance results of Schemes 1-3

Capacity of WTs (MW)	Energy procurement cost ($)			Total operation cost ($)			Network loss (MW)			Voltage deviation (p.u.)		
	Scheme 1	Scheme 2	Scheme 3	Scheme 1	Scheme 2	Scheme 3	Scheme 1	Scheme 2	Scheme 3	Scheme 1	Scheme 2	Scheme 3
0.7	3580.521	3665.051	**3554.263**	**4373.375**	4395.285	4384.284	2.299	2.367	**2.201**	23.906	24.128	**22.506**
1.4	3033.666	3120.139	**3010.301**	**3826.274**	3850.203	3838.631	1.969	2.001	**1.901**	**20.298**	20.446	20.653
2.1	2488.258	2572.589	**2461.641**	**3280.374**	3305.146	3291.548	1.712	1.796	**1.687**	**23.321**	25.777	24.159
2.8	1940.852	2025.536	**1915.582**	**2733.121**	2755.984	2744.899	**1.549**	1.620	1.581	22.254	21.431	**19.821**
3.5	1395.126	1480.573	**1370.031**	**2185.158**	2210.529	2200.031	**1.507**	1.591	1.554	24.241	**23.451**	23.601
4.2	846.956	933.631	**821.353**	**1640.585**	1664.961	1650.912	**1.544**	1.589	1.604	27.061	**23.721**	26.331
4.9	300.126	385.767	**275.357**	**1090.961**	1116.215	1107.011	**1.695**	1.716	1.750	25.796	**24.926**	27.157

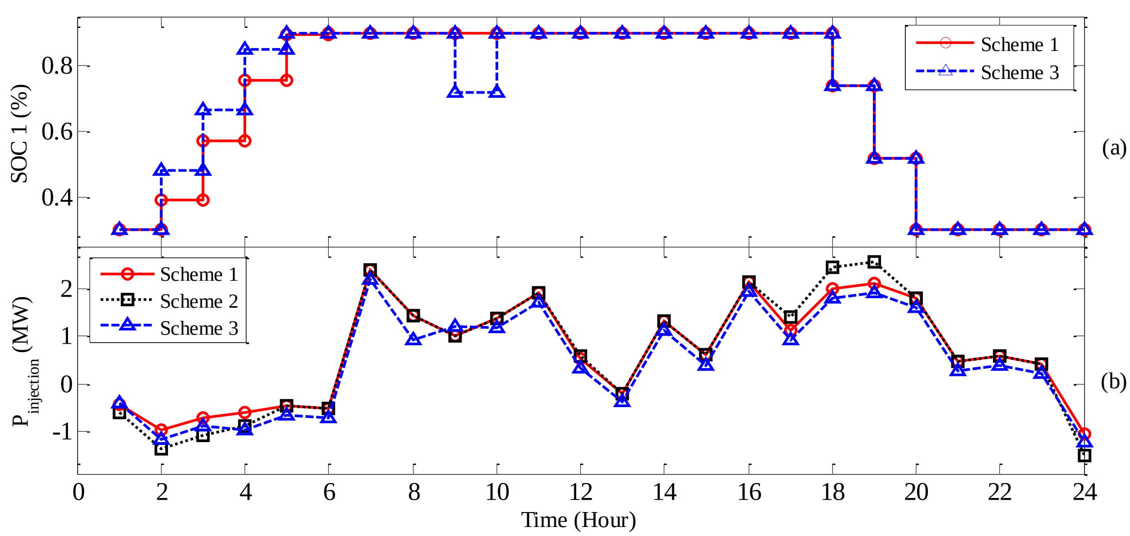

Fig. 7 The curves of the SOC of ESS 1 and energy procurement in Schemes 1-3: (a) SOC; (b) Injection from main gird.

The comparative simulations were performed under different penetration levels of wind energy to investigate the superiority of the proposed method. Table 3 exhibits the comparative results of Schemes 1-3 on network loss, energy procurement cost, voltage quality, and total operation cost, with the increase in the installed capacity of WTs from 0.7 MW to 4.9 MW. It can be seen from Fig. 6 that the wind generation is higher than the load demand during off-peak hours and lower than the load demand during on-peak hours. With the increase in the penetration level of WTs, the ESS in Schemes 1 and 3 can store the wind energy in excess of the load demand, and makes it accessible for later release during the peak price hours for the economic profit to reduce the energy procurement cost, as shown in Fig. 7. Consequently, the energy procurement cost in Scheme 2 without ESSs is higher than those in Schemes 1 and 3 under all the scenarios of wind penetration levels. From Table 3, with the increase of wind energy capacity, the energy procurement cost and total operation cost in Schemes 1-3 decrease gradually. On the other hand, since the ESS energy loss and degradation cost is not considered in Scheme 3, the charging/discharging actions of ESSs in Scheme 3 are more frequent than the other two schemes. For instance, during the period of hours 8-10 in Fig. 7(a), a reversal charging/discharging action is implemented for ESS 1 in Scheme 3. Hence, the frequent charging/discharging actions of ESSs in Scheme 3 can decrease the energy procurement cost, but it leads to the higher total operation cost compared with Scheme 1. It can also be concluded from the comparative results in Table 3 that the utilization of ESSs can enhance the economic performance for the distribution networks with wind energy. Furthermore, it can be found that the wind penetration level plays a major role in network loss. As shown in Table 3, the network loss in Schemes 1-3 decreases as the capacity penetration of WTs from 0.7 MW to 3.5 MW, and further increment in the wind energy capacity to 4.9 MW causes the reduction in the network loss. This is because the WTs can unload the power through the feeders and thus reduce the network losses. As the capacity of WTs gradually increases from 3.5 MW to 4.9 MW, the reverse power flow would be resulted in the radial distribution network to give rise to the excessive network losses and overheat feeders. In addition, the integration of different capacity of WTs would affect the voltage profile and load flow distribution of the distribution network, and then cause the change of voltage deviation performance.

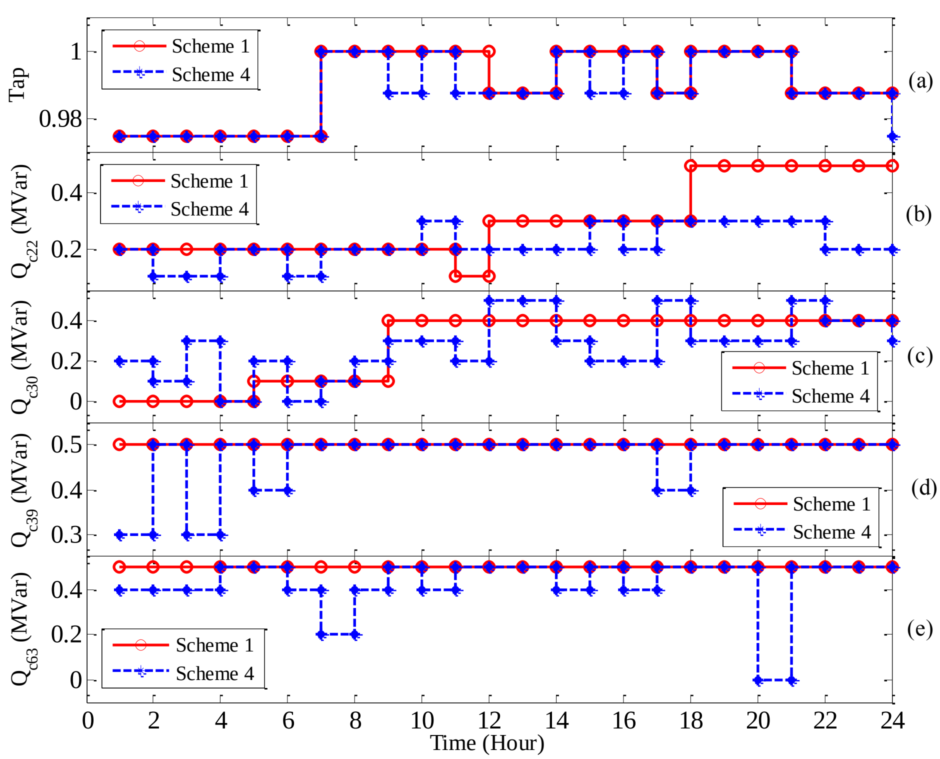

Fig. 8 The curves of OLTC Tap ratio and VAR outputs of shunt capacitors in Schemes 1 and 4: (a) OLTC tap ratio; (b) VAR output of CAP 22; (c) VAR output of CAP 30; (d) VAR output of CAP 39; (e) VAR output of CAP 63.

Table 4 Comparative results of the number of volt/var regulating actions in Schemes 1 and 4

Regulating No.	OLTC	Cap 22	Cap 30	Cap 39	Cap 63
Scheme 1	**8**	**4**	**2**	**1**	**1**
Scheme 4	12	11	19	8	15

Fig.7 illustrates the SOC curve of ESS 1 and the plot of energy procurement in Schemes 1-3 under the wind energy capacity of 3.5 MW. It can be found from Fig. 7 that the ESSs in Schemes 1 and 3 can be utilized for peak shaving and load leveling compared with Scheme 2, and the ESS degradation cost and energy loss cost in Scheme 3 could not be covered by the profits from the energy procurement of bidirectional power flow. Moreover, Fig. 8 shows the scheduling curves of volt/var control devices with Schemes 1 and 4 under the wind energy capacity of 3.5 MW. The scheduling results of OLTC tap ratio over the 24-hour period are shown in Fig. 8(a), and the optimized outputs of shunt capacitors at buses 22, 30, 39 and 63 are shown in Fig. 8(b)-(e). The numbers of regulating actions of OLTC and shunt capacitors over the entire 24-hour period are shown in Table 4. It is clear to see from Table 4 and Fig. 8 that, compared with Scheme 4, Scheme 1 with the objective function of CACDs can greatly decrease the maneuvering operations of the volt/var control devices. As a results, this reduction in the CACDs and ESS degradation cost would give opportunities for smart distribution networks to operate more efficiently, and less maneuvering cost, less wear-and-tear, and further savings on energy would be expected.

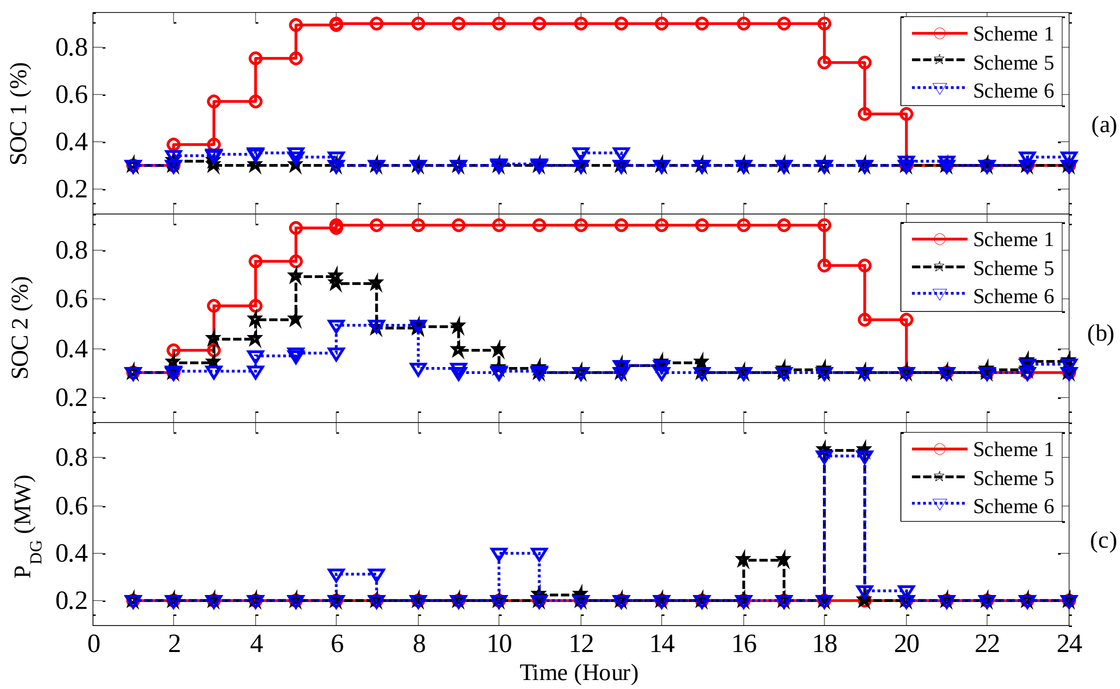

Fig. 9 The curves of the SOC of ESSs and outputs of DGs in Schemes 1, 5 and 6:

(a) SOC of ESS 1; (b) SOC of ESS 2; (c) DG power generation

Tables 5 and 6 list the comparative results of Schemes 1, 5 and 6 on total operation cost, network loss, demand consumption, CACDs, total energy consumption, and voltage quality, with the increase in the installed capacity of WTs from 0.7 MW to 4.9 MW. Fig.9 illustrates the SOC curves of ESSs and outputs of DGs in Schemes 1, 5 and 6 under the wind energy capacity of 3.5 MW. It can be found from the comparative results that the proposed two-stage framework in Scheme 1 implements the optimal economic generation scheduling for ESSs and DG, as shown in Fig.9, and thus can exhibit the superior performance on the total operation cost. Meanwhile, with the increasing penetration levels of grid-integrated WTs, Scheme 1 performs better with the other schemes on the network loss, demand consumption, CACDs, total energy consumption and voltage profile, and thus further confirms the effectiveness and validity of the proposed method for energy conservation with voltage reduction.

Table 5 Comparative performance results of Schemes 1 and 5

Capacity of WTs (MW)	Total operation cost ($)		Network loss(MW)		Demand consumption (MW)		CACDs (MW)		Total energy consumption (MW)		Voltage deviation (p.u.)	
	Scheme 1	Scheme 5	Scheme 1	Scheme 5	Scheme 1	Scheme 5	Scheme 1	Scheme 5	Scheme 1	Scheme 5	Scheme 1	Scheme 5
0.7	**4373.375**	4683.467	2.299	**2.231**	**70.110**	70.136	0.178	**0.122**	72.587	**72.489**	23.906	**23.591**
1.4	**3826.274**	3998.156	1.969	**1.901**	**70.169**	70.204	**0.162**	0.176	**72.230**	72.281	**20.298**	23.797
2.1	**3280.374**	3501.116	1.712	**1.670**	**70.081**	70.386	**0.154**	0.154	**71.947**	72.21	23.321	**22.301**
2.8	**2733.121**	2907.621	**1.549**	1.566	**70.218**	70.456	0.180	**0.154**	**71.947**	72.176	**22.254**	22.206
3.5	**2185.158**	2370.596	**1.507**	1.545	**70.406**	70.661	**0.122**	0.136	**72.035**	72.342	24.241	**22.284**
4.2	**1640.585**	1801.171	**1.544**	1.671	**70.496**	70. 681	**0.142**	0.152	**72.182**	72.504	27.061	**19.905**
4.9	**1090.961**	1301.465	**1.695**	1.775	**70.673**	70.891	**0.122**	0.22	**72.490**	72.886	**25.796**	27.904

Table 6 Comparative performance results of Schemes 1 and 6

Capacity of WTs (MW)	Total operation cost ($)		Network loss(MW)		Demand consumption (MW)		CACDs (MW)		Total energy consumption (MW)		Voltage deviation (p.u.)	
	Scheme 1	Scheme 6	Scheme 1	Scheme 6	Scheme 1	Scheme 6	Scheme 1	Scheme 6	Scheme 1	Scheme 6	Scheme 1	Scheme 6
0.7	**4373.375**	4786.771	**2.299**	2.405	**70.110**	70.161	**0.178**	0.194	**72.587**	72.760	23.906	**23.451**
1.4	**3826.274**	4081.656	**1.969**	1.991	**70.169**	70.255	**0.162**	0.188	**72.230**	72.434	20.298	**20.167**
2.1	**3280.374**	3705.011	**1.712**	1.904	**70.081**	70.333	**0.154**	0.170	**71.947**	72.407	**23.321**	25.045
2.8	**2733.121**	2967.135	**1.549**	1.696	**70.218**	70.405	**0.180**	0.186	**71.947**	72.287	22.254	**21.999**
3.5	**2185.158**	2428.894	**1.507**	1.587	**70.406**	70.659	**0.122**	0.16	**72.035**	72.406	24.241	**21.007**
4.2	**1640.585**	1990.172	**1.544**	1.766	**70.496**	70.736	**0.142**	0.164	**72.182**	72.666	27.061	**21.366**
4.9	**1090.961**	1380.655	**1.695**	1.861	**70.673**	70.801	**0.122**	0.210	**72.490**	72.872	**25.796**	26.526

A comparative study of the average computation time over 10 independent runs for different schemes is given in Table 7, and all the algorithms in Schemes 1-6 were implemented on a personal computer with 4-GHz Intel Core i7 CPU and 8GB RAM. It is quite evident that the proposed two-stage method in Schemes 1-4 requires less execution time than that of the other schemes, and thus demonstrates its high computational efficiency. Moreover, in order to further assess and compare the maximum penetration level of wind energy in the studied distribution network with all the schemes, the comparative performances of wind energy accomodation were investigated under the wind energy capacity of 13 MW, as shown in Table 8. With the grid-integration of large-capacity wind energy, the wind curtailment will be implemented in order to avoid any violation of voltage and thermal loading constraints, and WTs would be forced to decrease their outputs or disconnect from the distribution network when the corresponding nodal voltage or branch power flow drops or raises beyond the lower or upper limits. In this study, the wind generation outputs were curtailed with a step size of 0.1 MW in each WT once any violation of network constraint occurred, and hence the feasible decision solutions of all the schemes could be obtained through the continuous execution of wind curtailment

[28, 37]. It can be found from Table 8 that the proposed two-stage method in Scheme 1 can facilitate the accommodation of higher wind energy penetration compared with other schemes.

Table 7 Average computation time of different schemes

Performance	Scheme 1	Scheme 2	Scheme 3	Scheme 4	Scheme 5	Scheme 6
Average computation time (s)	791.120	**790.710**	790.830	791.250	830.123	14090.606

Table 8 Wind energy accommodation with different schemes

Performance	Scheme 1	Scheme 2	Scheme 3	Scheme 4	Scheme 5	Scheme 6
Wind energy accommodation (%)	**94.6**	93.8	93.8	94.6	93.1	89.2

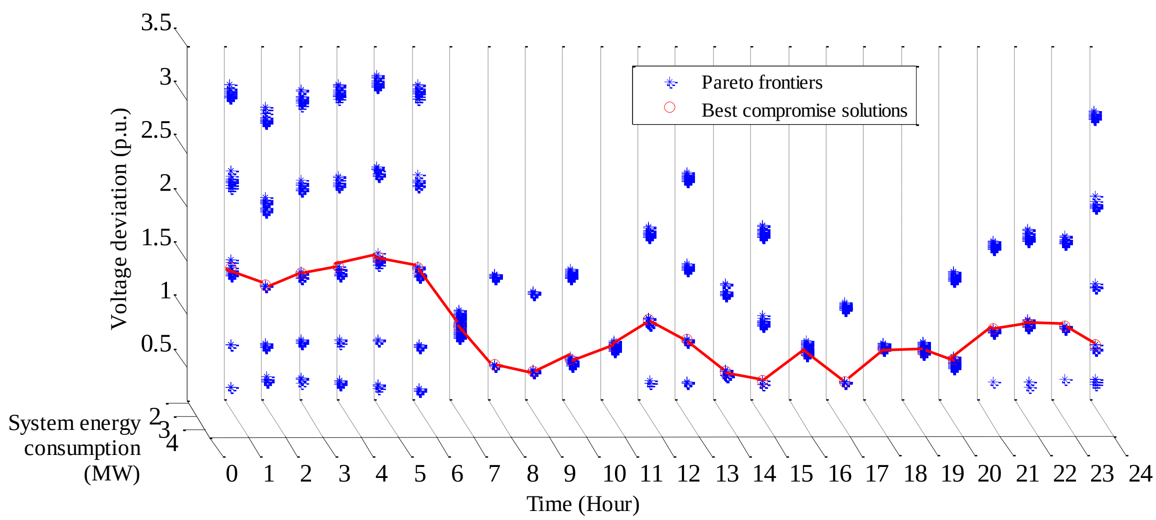

Fig. 10 The plots of Pareto frontiers and the best compromise solutions with Scheme 1 for 24-hour scheduling

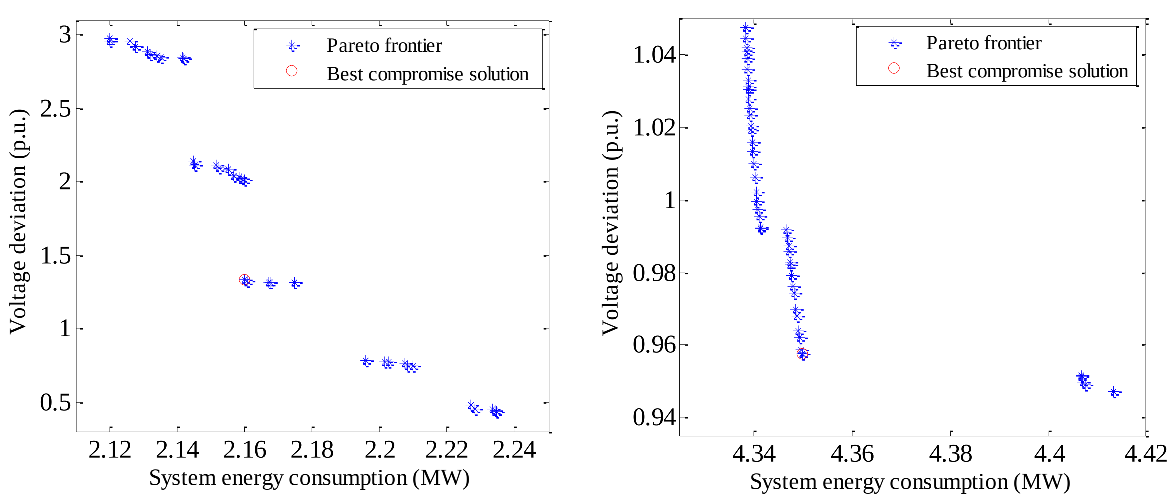

(a) (b)

Fig. 11 The plots of selected Pareto frontiers with Scheme 1 at: (a) hour 2; (b) hour 19.

In summary, the Pareto frontiers with the best compromise solutions resulted from the 24-hour VVO of Scheme 1 under the wind energy capacity of 3.5 MW are shown in Fig. 9, and the Pareto solution set of the proposed bi-objective VVO in each hour can also be obtained. Fig. 10 further plots the Pareto frontier at hour 2 (the period with maximum wind energy) and hour 19 (the period with peak load demand), and the best compromise solution in each Pareto frontier at each hour can be identified using the fuzzy decision making method in (34)-(35).

Moreover, three previous methods, including NSGA-II [17], multiobjective θ-smart bacterial foraging algorithm (Mθ-SBFA) [19], and modified teaching-learning-algorithm (MTLA) [23], were further performed to solve the volt/var management problem and compared with the proposed two-stage method. The parameter settings of the three methods can be obtained from [17, 19, 23]. All the methods were implemented over 10 independent runs, and the resulted sets of nondominated solutions are then combined and ranked by dominance comparisons to yield the best solution of each method. Table 9 provides the comparative results of the proposed two-stage method and the three methods on total operation cost, network loss, demand consumption, CACDs, total energy consumption, and voltage quality, under the wind energy capacity of 3.5 MW. The resulting statistics demonstrated that, due to the optimal coordinated scheduling of ESS, DG, and volt/var control devices across multiple time horizons, the proposed two-stage method can outperform the earlier methods and provide the best overall performance.

Table 9 Comparative performance results of different methods

Method	Total operation cost ($)	Network loss(MW)	Demand consumption (MW)	CACDs (MW)	Total energy consumption (MW)	Voltage deviation (p.u.)
Proposed method	**2185.158**	**1.507**	**70.406**	**0.122**	**72.035**	24.241
NSGA-II [17]	2290.196	1.599	70.505	0.136	72.140	**22.240**
Mθ-SBFA [19]	2358.094	1.553	70.516	0.140	70.209	23.548
MTLA [23]	2300.165	1.533	70.485	0.142	72.16	25.413

5. Conclusion

The integration of wind energy in distribution networks has a significant impact on both voltage quality and network loss due to the small X/R ratio and radial configuration, and this paper proposes a two-stage framework to facilitate the accommodation of high wind energy penetration. The main contributions of the proposed approach are summarized as follows: 1) A two-stage stochastic scheduling framework is proposed for the volt/var management problem to coordinately schedule ESS, DG, and volt/var control devices across multiple time horizons for the improvement on the wind energy accommodation capability; 2) In order to yield the economic benefits, the reverse power flow with coordinated ESS scheduling scheme is integrated to accommodate the large-capacity wind energy while considering the degradation cost and energy loss cost of ESS; 3) A multiobjective VVO model is proposed for high renewable-penetrated distribution networks with the consideration of the CACDs and voltage-based exponential load models.

Comparative studies have demonstrated the superiority of proposed approach on various performance objectives. The simulation results over a 24-hour period confirmed that the network loss, VD, CACDs, demand consumption, and operation cost can be effectively reduced under various penetration levels of wind energy, and the excessive operational actions on volt/var control devices and ESS can also be avoided. Furthermore, it can be found that due to the high energy loss and degradation cost, the ESS tends to participate in the charging/discharging scheduling for economic profits during the large peak-valley energy price difference. Further research would focus on the application of proposed approach in principle to the unbalanced three-phase distribution networks with stochastic RESs.

Acknowledgements

The authors gratefully acknowledge the support of the National Natural Science Foundation of China (51507056), the China Postdoctoral Science Foundation under Grant 2016M590737, the Hunan Natural Science Foundation of China (2017JJ3019), and The Hong Kong Polytechnic University under Project K-ZPB6.

References

[1] Tabatabaee S, Mortazavi S S, Niknam T. Stochastic scheduling of local distribution systems considering high penetration of plug-in electric vehicles and renewable energy sources. Energy 2016; 121: 480–490.

[2] Ishugah T F, Li Y, Wang R Z, et al. Advances in wind energy resource exploitation in urban environment: A review. Renew Sustain Energy Rev 2014; 37: 613-626.

[3] Onar S C, Oztaysi B, Otay İ, et al. Multi-expert wind energy technology selection using interval-valued intuitionistic fuzzy sets. Energy 2015; 90: 274-285.

[4] Zheng D, Eseye A T, Zhang J and Li H. Short-term wind power forecasting using a double-stage hierarchical ANFIS approach for energy management in microgrids. Protection and Control of Modern Power Systems 2017: 2: 10, DOI 10.1186/s41601-017-0041-5.

[5] IRENA. Renewable energy capacity statistics 2016. International Renewable Energy Agency; 2016.

[6] Zhang L, Zhou P, Newton S, et al. Evaluating clean energy alternatives for Jiangsu, China: An improved multi-criteria decision making method. Energy 2015; 90: 953-964.

[7] Goop J, Odenberger M, Johnsson F. Distributed solar and wind power–Impact on distribution losses. Energy 2016; 112(1): 273-284.

[8] Ochoa L F, Padilha-Feltrin A, Harrison G P. Time-series-based maximization of distributed wind power generation integration. IEEE Trans Energy Convers 2008; 23(3): 968-974.

[9] Atwa Y M, El-Saadany E F, Salama M M A, et al. Optimal renewable resources mix for distribution system energy loss minimization. IEEE Trans Power Syst 2010; 25(1): 360-370.

[10] Salih S N, Chen P, Carlson O, et al. Optimizing wind power hosting capacity of distribution systems using cost benefit analysis. IEEE Trans Power Del 2014; 29(3): 1436-1445.

[11] Salih S N, Chen P, Carlson O. The effect of wind power integration on the frequency of tap changes of a substation transformer. IEEE Trans Power Syst 2013; 28(4): 4320-4327.

[12] Niknam T. A new approach based on ant colony optimization for daily volt/var control in distribution networks considering distributed generators. Energy Convers Manage 2008; 49(12): 3417-3424.

[13] Zhou B, Chan K W, Yu T, et al. Strength Pareto multigroup search optimizer for multiobjective optimal reactive power dispatch. IEEE Trans Ind Inform 2014; 10(2): 1012-1022.

[14] Niknam T. A new HBMO algorithm for multiobjective daily volt/var control in distribution systems considering distributed generators. Appl Energy 2011; 88(3): 778-788.

[15] de Souza B A, de Almeida A M F. Multiobjective optimization and fuzzy logic applied to planning of the volt/var problem in distributions systems. IEEE Trans Power Syst 2010; 25(3): 1274-1281.

[16] Wang Z, Wang J, Chen B, et al. MPC-based voltage/var optimization for distribution circuits with distributed generators and exponential load models. IEEE Trans Smart Grid 2014; 5(5): 2412-2420.

[17] Padilha-Feltrin A, Rodezno D A Q, Mantovani J R S. Volt-var multiobjective optimization to peak-load relief and energy efficiency in distribution networks. IEEE Trans Power Del 2015; 30(2): 618-626.

[18] Ahmadi H, Martí J R, Dommel H W. A framework for volt-var optimization in distribution systems. IEEE Trans Smart Grid 2015; 6(3): 1473-1483.

[19] Zare M, Niknam T. A new multi-objective for environmental and economic management of volt/var control considering renewable energy resources. Energy 2013; 55(15): 236-252.
[20] Zare M, Niknam T, Azizipanah-Abarghooee R, and Amiri B. Multi-objective probabilistic reactive power and voltage control with wind site correlations. Energy 2014; 66(4): 810-822.
[21] Xu Y, Dong Z Y, Zhang R, et al. Multi-timescale coordinated voltage/var control of high renewable-penetrated distribution systems. IEEE Trans Power Syst 2017; Published Online, DOI: 10.1109/TPWRS.2017.2669343.
[22] Malekpour A R, Niknam T. A probabilistic multi-objective daily volt/var control at distribution networks including renewable energy sources. Energy 2011; 36(5): 3477-3488.
[23] Niknam T, Zare M, Aghaei J. Scenario-based multiobjective volt/var control in distribution networks including renewable energy sources. IEEE Trans Power Del 2012; 27(4): 2004-2019.
[24] W. Price et al. Bibliography on load models for power flow and dynamic performance simulation. IEEE Trans Power Syst 1995; 10(1): 523–538.
[25] Singh R, Pal BC, Jabr RA. Distribution system state estimation through gaussian mixture model of the load as pseudo-measurement. IET Transmiss Distrib Gen 2010; 4(1): 50–59.
[26] Khodayar M E, Shahidehpour M, Wu L. Enhancing the dispatchability of variable wind generation by coordination with pumped-storage hydro units in stochastic power systems. IEEE Trans Power Syst 2013; 28(3): 2808-2818.
[27] Zhou B, Liu X, Cao Y, et al. Optimal scheduling of virtual power plant with battery degradation cost. IET Transmiss Distrib Gen 2016; 10(3): 712-725.
[28] Gabash A, Li P. Flexible optimal operation of battery storage systems for energy supply networks. IEEE Trans Power Syst 2013; 28(2): 2788-2797.
[29] Albu M, Sanduleac M, Stanescu C. Syncretic use of smart meters for power quality monitoring in emerging networks. IEEE Trans Smart Grid 2016; Published Online, DOI: 10.1109/TSG.2016.2598547.
[30] E. R. Richard. GAMS-a user's guide. Washington D.C. GAMS Development Corporation 2015.
[31] Robič T, Filipič B. DEMO: Differential evolution for multiobjective optimization. Int Conf Evol Multi-Criterion Optim 2005; 3410: 520-533.
[32] Abido M A. Multiobjective evolutionary algorithms for electric power dispatch problem. IEEE Trans Evol computation 2006; 10(3): 315-329.
[33] Baran M, Wu F. Optimal capacitor placement on radial distribution systems. IEEE Trans Power Del 1989; 4(1): 725-734.
[34] Ma X, Wu Y, Fang H, et al. Optimal sizing of hybrid solar-wind distributed generation in an islanded microgrid using improved bacterial foraging algorithm. Proceedings of the CSEE 2011; 31(25): 17-24.
[35] Zhang Y, Ren Z. Optimal reactive power dispatch considering costs of adjusting the control devices. IEEE Trans Power Syst 2005; 20(3): 1349-1356.
[36] Time-of-Use Prices, 2016. [Online]. Available: http://www.ieso.ca/imoweb/siteshared/tou_rates.asp?sid=ic/.
[37] Doherty R, Bryans L, Gardner P, et al. Wind penetration studies on the island of Ireland. Wind Eng 2004; 28(1): 27-41.